Journal of Liposome Research

ISSN: 0898-2104 (Print) 1532-2394 (Online) Journal homepage: www.tandfonline.com/journals/ilpr20

# Triple co-culture spheroid models of lung and ovarian carcinoma cell lines for the *in vitro* testing of antitumor liposomes

Shrey Shah, Yongwoon Kim, Rock Pulak & Gerard G. M. D'Souza

**To cite this article:** Shrey Shah, Yongwoon Kim, Rock Pulak & Gerard G. M. D'Souza (05 Jun 2025): Triple co-culture spheroid models of lung and ovarian carcinoma cell lines for the *in vitro* testing of antitumor liposomes, Journal of Liposome Research, DOI: 10.1080/08982104.2025.2514850

**To link to this article:** https://doi.org/10.1080/08982104.2025.2514850

Published online: 05 Jun 2025.

JOURNAL OF LIPOSOME RESEARCH
https://doi.org/10.1080/08982104.2025.2514850

Taylor & Francis
Taylor & Francis Group

RESEARCH ARTICLE



# Triple co-culture spheroid models of lung and ovarian carcinoma cell lines for the *in vitro* testing of antitumor liposomes

Shrey Shah[a], Yongwoon Kim[b], Rock Pulak[b] and Gerard G. M. D'Souza[a]

[a]Department of Pharmaceutical Sciences, School of Pharmacy-Boston, MCPHS University, Boston, MA, USA; [b]Union Biometrica Inc., Holliston, MA, USA

**ABSTRACT**

Tumor cells cultured as spheroids have been shown to be superior to tumor cells cultured in monolayers as *in vitro* models of solid tumors because they exhibit features of the tumor microenvironment (TME) such as cell-cell interactions, extracellular matrix and diffusional gradients. However, spheroids composed solely of tumor cells, i.e. monoculture spheroids, still lack the non-tumor cell components that contribute to additional *in vivo* TME complexity. This study, explored the development of triple co-culture spheroid models incorporating tumor cells, tissue specific fibroblasts, and endothelial cells to mimic more of the features of the *in vivo* TME. Using a modified liquid overlay technique, triple co-culture spheroids were successfully generated for both drug resistant lung tumor cells as well as drug resistant ovarian tumor cells. The triple co-culture models exhibited several characteristics of *in vivo* tumors, including extracellular matrix (ECM) production and distinct spatial locations of cell types. Notably, fibroblasts remained in the core as the spheroid grew, while endothelial cells were found in the core only in the presence of fibroblasts. A liposomal formulation previously shown in monolayer cultures to have selective toxicity toward multiple drug resistant tumor cell types was significantly less toxic and showed composition-dependent levels of toxicity in spheroid cultures with multiple cell types. These findings demonstrate that triple co-culture spheroids can serve as *in vitro* models that more closely mimic *in vivo* tumor characteristics to facilitate the optimization of antitumor therapies prior to *in vivo* testing.

**HIGHLIGHTS**

- Development of spheroid models of human lung and ovarian carcinoma incorporating drug-resistant tumor cells, tissue specific fibroblasts, and endothelial cells.
- Spheroids demonstrated key features of tumor biology, including avascular growth, extracellular matrix production, and distinct spatial arrangement of cell types.
- Spheroid response to potential antitumor liposomal preparation showed differences not apparent in testing on monolayer cultures or monoculture spheroids.

**ARTICLE HISTORY**
Received 19 February 2025
Revised 23 May 2025
Accepted 26 May 2025

**KEYWORDS**
Multicellular spheroid; tumor microenvironment; extra cellular matrix; Spheroid flowcytometry; Cellular migration

## Introduction

*In vitro* disease models are an important tool in the development and testing of treatment approaches [1]. The current *in vitro* testing approach for tumor therapies most commonly relies on cell cultures of tumor cells grown in monolayers [1–3]. These cell cultures lack many of the characteristics of tumor physiology and are often not a sufficiently discriminating test of delivery strategies aimed at improving tumor accumulation of anticancer agents [4,5]. There remains a need for *in vitro* tumor models that more closely mimic the tissue architecture and microenvironment of *in vivo* tumors to enable more rigorous testing of tumor delivery strategies before testing in *in vivo* models. In this context, spheroid culture has gained prominence as a potential improvement over monolayer culture [6,7]. Spheroids result from the growth of tumor cells in large aggregates with intracellular interactions and structural elements that more closely resemble *in vivo* tumors [8,9]. Spheroid culture also results in gradients of oxygen, nutrients, and metabolites in the spheroid mass [9,10]. These gradients are an important aspect necessary for the establishment of features such as hypoxic cores, differential proliferation zones, and regions of necrosis that are hallmarks of the microenvironment of *in vivo* solid tumors [9–11].

Since their introduction in the 1970s, spheroids have been utilized to provide valuable insights into tumor biology, particularly in understanding cell-cell interactions, proliferation, and responses to anticancer therapies [12–14]. However, the majority of these studies utilized spheroids comprised of tumor cells only [15–17]. I*n vivo* tumors are not clusters of tumor cells alone; they are dynamic and heterogeneous tissues composed of various cell types, including fibroblasts, endothelial cells and immune cells [18,19]. The non-tumor cells play essential roles in tumor development, progression, and stromal composition that affect the tumor response to therapy [18–20]. For instance, Cancer-associated fibroblasts (CAFs) are pivotal components of the tumor microenvironment, playing a crucial role in cancer progression [21]. Typically quiescent, these fibroblasts become activated in

**CONTACT** Gerard G. M. D'Souza gerard.dsouza@mcphs.edu Department of Pharmaceutical Sciences, School of Pharmacy-Boston, MCPHS University, Boston, MA, USA

response to signals from tumor cells and other elements within the microenvironment [21,22]. Once activated, CAFs secrete a wide array of signaling molecules, including growth factors, cytokines, chemokines, and ECM components, which collectively create a supportive niche for tumor development and progression [21–25]. A key function of CAFs is the remodeling of the extracellular matrix (ECM). By producing and reorganizing ECM proteins like collagen, fibronectin, and laminin, CAFs not only provide structural support to tumors but also enhance cancer cell migration and invasion—a process known as desmoplasia [26–29]. Endothelial cells, on the other hand, are integral to angiogenesis, a process critical for tumor vascularization and nutrient supply. Angiogenesis is essential for tumor growth, as it delivers the necessary oxygen and nutrients to sustain the expanding tumor mass [30]. Endothelial cells respond to pro-angiogenic signals such as vascular endothelial growth factor (VEGF), which are secreted by both tumor cells and CAFs [31,32]. Beyond forming new blood vessels, endothelial cells can influence the behavior of nearby tumor cells, enhancing their invasive potential and facilitating metastasis to distant sites [33–35]. Endothelial cells also contribute to forming a barrier that can affect the infiltration and effectiveness of immune cells and therapeutic agents within the tumor [36,37]. Finally, depending on their type and activation state, the immune cells within the tumor microenvironment can either suppress or promote tumor progression [18]. Therefore, spheroids composed solely of tumor cells cannot be expected to suitably mimic the complex mechanisms of drug resistance, invasion, and metastasis observed *in vivo* to serve as adequate representations of *in vivo* tumors.

This study focused on the development of spheroids of drug-resistant lung and ovarian carcinoma cells that include fibroblasts and endothelial cells in order to create an *in vitro* tumor model that is a better representation of the *in vivo* tumor microenvironment (TME). The increased similarity to the *in vivo* tumor environment should help to improve the stringency of *in vitro* drug testing. To this end, a previously characterized liposomal preparation that has shown drug-resistant tumor cell-specific toxicity was used as a preliminary test of the new model [38,39]. The low toxicity observed in the spheroid models tested supports the hypothesis that spheroids comprised of multiple sub populations of cells will serve as a better test of potential *in vivo* effect than monolayer cultures.

## Materials

Doxorubicin-resistant human lung tumor cell line (H69/AR, #CRL-11351) was purchased from American Type Culture Collection (ATCC; Manassas, VA, USA). Doxorubicin-resistant human ovarian tumor cell line (A2780/ADR, #3112520) was purchased from Sigma Aldrich (St. Louis, MO). Human Lung Fibroblasts (HLF, #cAP-0033) and their green fluorescent protein expressing (#cAP-0033GFP) variant, Human Umbilical Vein Endothelial Cells (HUVEC, #cAP-0001) and their red fluorescent protein expressing variant (#cAP-0001RFP) were purchased were purchased from Angio-Proteomie (Boston, MA). Human Ovarian Fibroblasts (HOF, #7330) were purchased form Science cell research laboratories (Carlsbad, CA). Roswell-Park medium (RPMI 1640) used to culture tumor cell lines, fibroblast growth medium required to culture fibroblast cells, and endothelial growth medium required to culture HUVECs were purchased from the companies from which the cell lines were purchased. Fetal Bovine Serum (FBS), Phosphate Buffered Saline (PBS) pH 7.4, and Hoechst dye were purchased from Thermo Fisher Scientific (Waltham, MA, USA). Trypsin-EDTA and Penicillin-Streptomycin solutions were purchased from Corning (New York City, NY, USA). Paraplast-plus embedding agent and standard cassettes for histology were purchased from VWR (Radnor, PA, USA). Standard Tissue-Tek cryo mold was purchased from Electron Microscopy Sciences (Hatfield, PA, USA). Histological grade xylene and alcohol were purchased from Fischer Scientific (Waltham, MA, USA). Bovine Serum Albumin, glycine, and 0.1% Triton-X were purchased from Boston Bio Products (Ashland, MA, USA). Anti-Fibronectin antibody (#ab2413), Anti-Collagen I antibody (#ab138492), Goat Anti-Rabbit IgG H&L (#ab150115, Alexa Fluor® 647), Goat Anti-Rabbit IgG H&L (#ab150077, Alexa Fluor® 488), Antigen Retrieval Buffer (Tris-EDTA Buffer, pH 9.0), Antigen retrieval Buffer (Citrate Buffer, pH 6.0) and Goat Serum were purchased from Abcam (Waltham, MA, USA). Adenosine 5′-triphosphate dipotassium salt hydrate was purchased from Sigma Aldrich (St. Louis, MO, USA). Cell Titer-Glo® 3D Cell Viability Assay and Cell Titer 96® Aqueous One Solution Cell Proliferation Assay reagent was purchased from Promega (Madison, WI, USA, USA).

## Methods

### Cell culture

H69/AR and A2780/ADR were cultured using RPMI 1640 medium supplemented with 1% penicillin-streptomycin (10000 U/mL) with 20 and 10% (FBS), respectively. HLF and HOF were cultured using a fibroblast growth medium supplemented with 1% penicillin-streptomycin (10000 U/mL) with 10% FBS. Additionally, 1% fibroblast growth serum was added to the media used to culture HOF. HUVECs were cultured using an endothelial growth medium supplemented with 10% FBS and 1% penicillin-streptomycin (10000 U/mL). Cells were cultured using a standard protocol provided by the manufacturer in T-75 flasks maintained at 37 °C, 5% $CO_2$ environment. The cells were passaged when a flask was 80% confluent. Cells were discarded after 30 passages for tumor cell lines, 10 passages for fibroblast, and 20 passages for endothelial cells.

### Spheroid production

Spheroids were produced using a liquid-overlay technique on agar surfaces. Briefly, 1% agar solution in serum-free media was coated in each well of a 96-well plate. Cell suspensions of desired concentration were plated in each well and the plates were centrifuged using a plate centrifuge (Thermo Fischer Marathon 3000R) at 500 × g. The number of cells

plated and the centrifugation time were optimized for each cell line. Then the plates were placed in an incubator maintaining a temperature at 37 °C, 5% $CO_2$ environment.

### Cell viability measurement

For monolayer cultures, cells were seeded in a 96-well plate such that they would reach ~70% confluency the next day. On reaching the desired confluency, STPP liposomes were added at 80 µM concentrations in 100 µL of media per well and further incubated for 5 or 24 h. After the incubation for the required time, preparation along with the media were removed and replaced with 100 µL media containing CellTiter 96® Aqueous one solution cell proliferation assay reagent equivalent to 10 µL/well. The plate was further incubated for 1 h followed by measurement of absorbance using a BioTek Synergy HTX Multimode Reader (Agilent, Santa Clara, CA, USA).

Individual spheroids ($n = 4$) were harvested from the round bottom wells and transferred in a microtube using a pipette. The culture medium was carefully removed, spheroids were washed with PBS (to remove any extracellular ATP and then redispersed in complete media. The spheroid suspension was then transferred into white-opaque 96-well plates (Thermo Fischer Scientific, Waltham, MA, USA) and an appropriate volume of Cell Titer-Glo® 3D reagent was added into each well. Plates were protected from light and gently shaken for 2 min at room temperature to induce spheroid lysis. Samples were incubated for an additional 25 min in the dark, at room temperature, to stabilize the bioluminescent signal, which was then recorded using a benchtop plate reader (BioTek, Winooski, VT, USA). The ATP concentration in each sample was quantified by using a calibration curve based on rATP standards according to the manufacturer's instructions.

### Spheroid size measurement

At predetermined time points, brightfield microscopy images of spheroids (n=10) were taken using a Keyence BZ-X800E microscope (Keyence, Woburn, MA, USA). The manufacturer's analysis software for the BZ-X800E was used measure the diameter of imaged spheroids.

### Spheroid immunohistochemistry

At predetermined time points—day 6 for co-cultured lung tumor spheroids and day 4 for co-cultured ovarian tumor spheroids—the spheroids were carefully removed from the 96-well plates and fixed in 4% paraformaldehyde for 30 min. Following fixation, the spheroids were washed three times with 1X PBS and subsequently embedded in Histogel™. The Histogel™-embedded spheroids were then transferred to tissue cassettes for processing. This processing involved sequential dehydration in graded ethanol solutions and clearing with xylene. To achieve paraffin infiltration, the tissue cassettes containing the Histogel™-embedded spheroids were incubated in molten paraffin overnight. The final embedding was performed by placing the Histogel™ in a mold, pouring additional paraffin over it, and allowing it to solidify on an ice bath.

Fixed paraffin-embedded samples were sectioned in 5 µm sections using a Leica SM2010R microtome, followed by deparaffinization in xylene and rehydration in sequentially decreasing ethanol concentrations. Before staining, to retrieve the antigens, sections were treated with either sodium citrate buffer, pH 6, or Tris-EDTA Buffer, pH 9.0 at 96 °C for 30 min. Next, samples were washed three times by immersing sections in PBS-Tween20 (PBS-T), pH 7.4, under agitation (60 rpm) for 5 min. To permeabilize the samples, sections were immersed in Triton-X (0.1% in PBS) at 60 rpm for 10 min and then again washed 3 times with PBS-Tween20. Before adding antibodies, samples were blocked with 4%BSA, 10% goat serum, and 0.3 M glycine solution. Primary human antibody (Anti-Fibronectin 1:200) or primary human antibody (Anti-Collagen 1:250) were added to the samples and incubated overnight, at 4 °C. Samples were washed three times and the secondary antibody (at 1:250 dilution) and counterstained with Hoechst dye (5 µM) in PBST (*v/v*) were incubated, in the dark, for 10 min at room temperature. Finally, sections were mounted with Aqua-Mount™ and imaged with a Keyence BZ-X800E microscope (Keyence, Woburn, MA, USA).

### Spheroid flow cytometry

The cellular composition of spheroids was analyzed using flow cytometry. Once the spheroids reached a diameter of 500 micrometers, eight spheroids were collected per sample in Eppendorf tubes. To achieve single-cell dissociation, 100 microliters of trypsin was added, followed by incubation at 37 °C for 30 min. The dissociated cells were then subjected to flow cytometric analysis. Endothelial cells, which inherently expressed red fluorescent protein, were detected in the red fluorescence channel, while fibroblasts, which expressed green fluorescent protein, were detected in the green fluorescence channel. Tumor cells did not express any fluorescent protein and were identified as nonfluorescent. A total of 5000 events were acquired per sample, and the proportions of red fluorescent, green fluorescent, and nonfluorescent populations were quantified to determine the cellular composition within the spheroids.

Whole spheroid analysis (n >200) was performed with a COPAS Vision large particle flow cytometer (Union Biometrica, Inc., Holliston, MA, USA). The flow cytometer was configured with a 1000 µm flow cell, capable of accommodating spheroids ranging from 15 to 850 µm in cross-sectional diameter. Spheroids were transferred from 96-well plates into 50 ml conical tubes containing 1X PBS to facilitate aspiration into the flow cell for analysis. The system utilized a 488 nm laser for object detection within the flow cell and excitation of GFP-labeled cells within spheroids, alongside a 561 nm laser for excitation of RFP-labeled cells within spheroids. Real-time imaging of spheroids within the flow cell was achieved through a 450 nm brightfield light, a 5× objective lens, and a Hamamatsu CMOS high-speed camera with a 1 µsec exposure time. Optical density (OD) and time of flight (TOF) were determined via a light-loss detector aligned with the laser

beam while fluorescence emission was captured orthogonally to the laser path using appropriate bandpass filters for GFP and RFP emissions. Fluorescence data are obtained as integral values, with more detailed analysis possible through the Profiler™ feature, which records intensities of fluorescence and OD signals along an object's length to allow for the identification of internal structures or patterns within the object.

### Liposome preparation

Liposomes with a total lipid concentration of 5 mg/mL were prepared using the thin film hydration method. Appropriate volumes of chloroform stock solutions of egg PC, cholesterol, and STPP were added to a 10 ml round bottom flask. A thin lipid film was obtained after chloroform's evaporation with a rotary evaporator's help under vacuum at 37 °C. The lipid film was then hydrated with 2 ml PBS pH 7.4 and was subjected to sonication for two 10-min periods with a resting interval of 1 min between the two sonication periods. Sonication was carried out using a Model 100 Sonic Dismembrator (Fischer Scientific, Waltham, MA, USA) with the round bottom flask immersed in an ice water bath. The particle size and zeta potential of the resulting liposomes were measured in a 90Plus Particle Size Analyzer (Brookhaven Instruments Corporation, Holtsville, NY, USA).

### Statistical analysis

Results are expressed as mean ± standard deviation of at least three independent experiments. All statistical analyses were performed using GraphPad Prism (GraphPad Software, San Diego, CA, USA). Statistical significance was analyzed either with Student's *t*-test or with a two-way analysis of variance (ANOVA) and Tukey *post-hoc* test, with the level of significance set at $p < 0.01$.

## Results

### Spheroid production and characterization

Figure 1(A) shows the successful formation of spheroids by H69/AR cells alone (monoculture) and when combined with HLF (co-culture) or HLF and HUVEC (triple co-culture). Figure 1(B) shows that A2780/ADR cells alone (monoculture) were unable to form spheroids but were able to form spheroids when combined with HOF (co-culture) or with HOF and HUVEC (triple co-culture). The spheroids shown were cultured following initial optimization of the minimum seeding density and ratio of the constituent cell lines to initiate spheroid formation within 24 h. For lung tumor spheroids, a seeding density of 5,000 total cells per well was sufficient across monoculture, co-culture, and triple co-culture setups. The optimal seeding cell ratio was 9:1 for H69/AR:HLF co-culture spheroids and 8:1:1 for H69/AR:HLF:HUVEC triple co-culture spheroids. The ovarian tumor spheroids required a slightly higher seeding density of 6,000 cells per well. The optimal seeding cell ratio was 26:3 A2780/ADR:HOF co-culture spheroids and 26:3:2 for A2780/ADR:HOF:HUVEC triple co-culture spheroids. All spheroids formed exhibited a spherical morphology allowing for diametric measurements as an indication of spheroid growth. Figure 1(C) shows the diametric measurements of H69/AR spheroids. The spheroids continued to increase in size over the observed period with monoculture H69/AR spheroids reaching a diameter of 800 µm, co-culture spheroids reaching 600 µm, and triple co-culture spheroids reaching 700 µm by day 10. Diametric measurements of A2780/ADR co-culture and triple-co-culture spheroids shown in Figure 1(D) also show that size increased over time but the overall growth pattern was more sigmoidal than the H69/AR spheroids.

ATP concentration was measured in spheroids to enable comparison of metabolic activity between spheroid types. As shown in Figure 1(E), H69/AR monoculture spheroids had significantly higher ATP concentrations compared to co-culture and triple co-culture spheroids on all days measured ($p < 0.01$ two-way ANOVA and Tukey's multiple comparison *post hoc* test). The ATP concentration also increased significantly over time for each type of H69/AR spheroid. Similarly, Figure 1(F) shows that A2780/ADR co-culture spheroids exhibited significantly higher ATP concentrations than triple co-culture spheroids across all time points ($p < 0.01$, two-way ANOVA and Tukey's multiple comparison *post hoc* test). ATP concentrations also increased significantly over time for all A2780/ADR spheroids ($p < 0.01$, two-way ANOVA and Tukey's multiple comparison *post hoc* test).

Immunohistochemistry was used to detect the presence of the major ECM components fibronectin and collagen in the spheroids. Figure 2(A,B) show representative epifluorescence micrographs of fibronectin and collagen staining. Figure 2(A) shows that H69/AR monoculture spheroids had little to no fibronectin, whereas co-culture spheroids showed high levels of fibronectin staining. Similar fibronectin levels were observed in A2780/ADR co-culture spheroids. Figure 2(B) shows that all spheroid types showed high levels of collagen staining.

Epifluorescence microscopy was then used to verify the presence of the different cell types in co-culture and triple co-culture spheroids. To this end, GFP expressing HLF and RFP expressing HUVEC variants were used to facilitate detection. Figure 3(A) shows that H69/AR:HLF co-culture spheroids had clear regions of green fluorescent staining while Figure 3(B) shows red fluorescent regions in H69/AR:HUVEC co-culture spheroids. As can be seen in Figure 3(C) H69/AR:HLF:HUVEC triple co-culture spheroids showed distinct green and red fluorescence. Red fluorescence from RFP expressing HUVECs was also seen in A2780/ADR:HOF:HUVEC triple co-culture spheroids as shown in Figure 3(D). The use of fluorescently labeled cell lines also facilitated flow cytometry analysis of cell ratios in the spheroids. Analysis of H69/AR:HLF co-culture and H69/AR:HLF:HUVEC triple co-culture spheroids dissociated on day 5 using trypsin and mild agitation indicated the H69/AR:HLF ratio was approximately 65%:35%, and the H69/AR:HLF:HUVEC ratio was approximately 60%:30%:10%. In A2780/ADR:HOF:HUVEC triple coculture spheroids the non-fluorescent to red fluorescent cell ratio was 90%:10%.

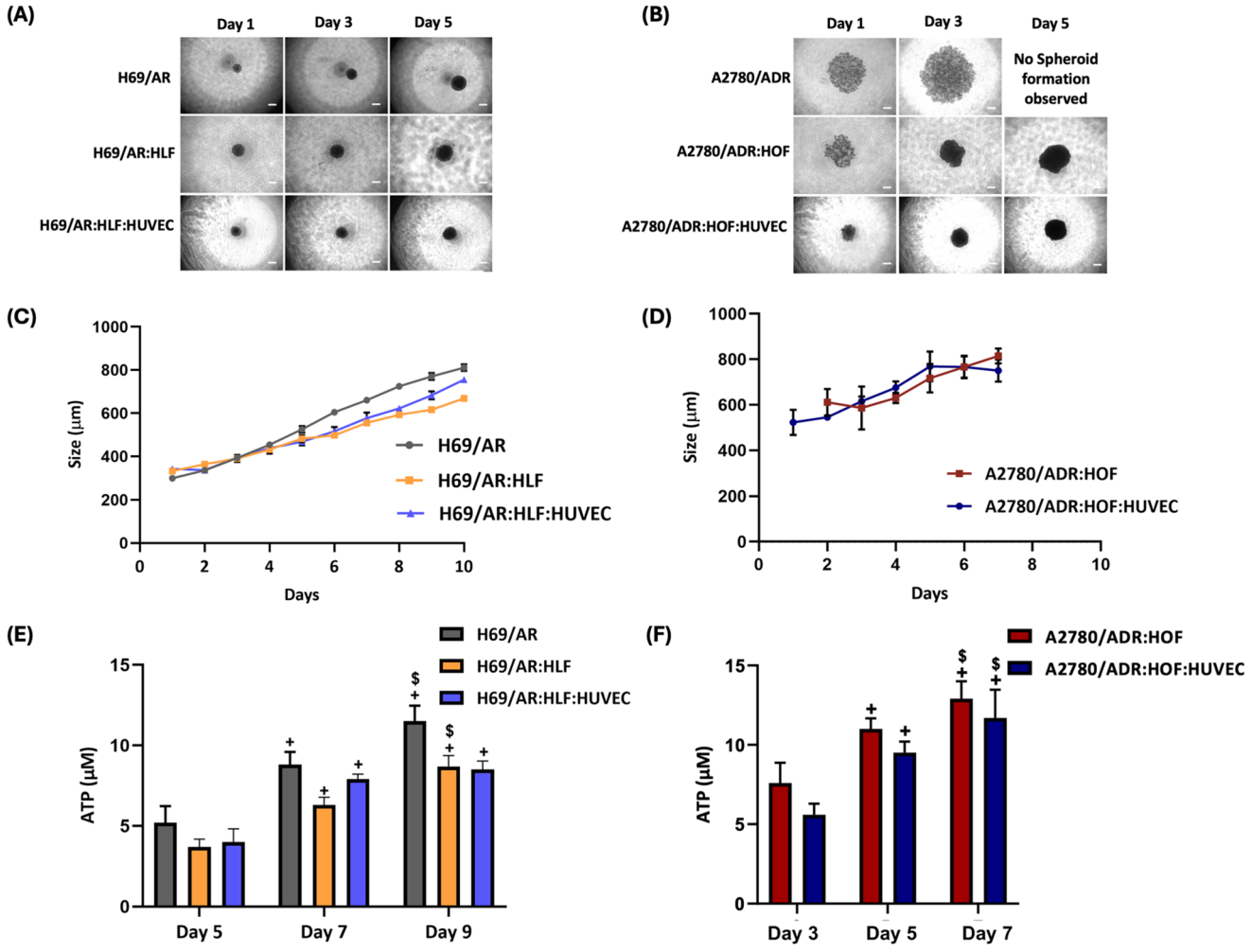


Figure 1. Characterization of spheroid growth and metabolic activity. Representative brightfield micrographs of (A) H69/AR monoculture, H69/AR:HLF co-culture, and H69/AR:HLF:HUVEC triple co-culture spheroids; (B) A2780/ADR monoculture, A2780/ADR:HOF co-culture and A2780/ADR:HOF:HUVEC triple co-culture spheroids. Scale bars represent 250 µm. Diametric measurements of monoculture, co-culture, and triple co-culture (C) H69/AR spheroids and (D) A2780/ADR spheroids. Data represented as mean ± standard deviation ($n = 4$). ATP concentration in monoculture, co-culture, and triple co-culture (E) H69/AR spheroids and (F) A2780/ADR spheroids. Data represented as mean ± standard deviation ($n = 10$). Two-way ANOVA, followed by Tukey's multiple comparison *post hoc* test. +$p < 0.01$ vs. day 5 for lung tumor and day 3 for ovarian tumor spheroids within respective groups. \$$p < 0.01$ vs. day 7 for lung tumor and day 5 for ovarian tumor spheroids within respective groups.

After initial optimization and analysis of the spheroids, the characteristics of whole H69/AR co-culture and triple co-culture spheroids were analyzed using a specialized large particle flow cytometer. Figure 4(A) shows time of flight (TOF) measurements of the spheroids. In this context, TOF represents the time the spheroid spends in the laser beam. A large spheroid will exhibit a long TOF to traverse the laser beam, while a small spheroid will have a shorter TOF across the laser beam. The 5-day old co-culture spheroids exhibited significantly higher TOF compared to 3-day old spheroids ($p < 0.01$, Student's *t*-test). The TOF for 5-day old triple co-culture spheroids was not significantly different than the TOF for 5-day old co-culture spheroids. Figure 4(B) shows optical density (OD) measurements that provide a measure of the density of the spheroids. The 5-day old co-culture spheroids had a significantly higher OD compared to 3-day-old co-culture spheroids ($p < 0.01$, Student's *t*-test). The OD values for 5-day old triple co-culture spheroids were similar to 5-day old co-culture spheroids.

The large particle flow cytometer also facilitates the simultaneous detection of OD and fluorescence emission signals across the spheroid mass. The OD signal shows the overall extent of the spheroid mass while the green fluorescent signal indicates the location of GFP expressing HLF cells and the red fluorescent signal indicates the location of RFP expressing HUVEC cells. Figure 4(C) shows that in the 3-day old co-culture spheroid, the green signal was distributed across most of the OD signal, while in the 5-day old co-culture spheroid, the green signal was more pronounced in the central region. In the 5-day-old triple co-culture spheroid both the green and red fluorescent signals remained pronounced in the central region and differed from each other only in magnitude.

The integral fluorescence to OD ratio is a quantitative measure of fluorescence localization. A higher ratio indicates an even distribution of fluorescent label throughout the spheroid, whereas a lower ratio suggests that the fluorescent label is localized in a discrete region. Figure 4(D)

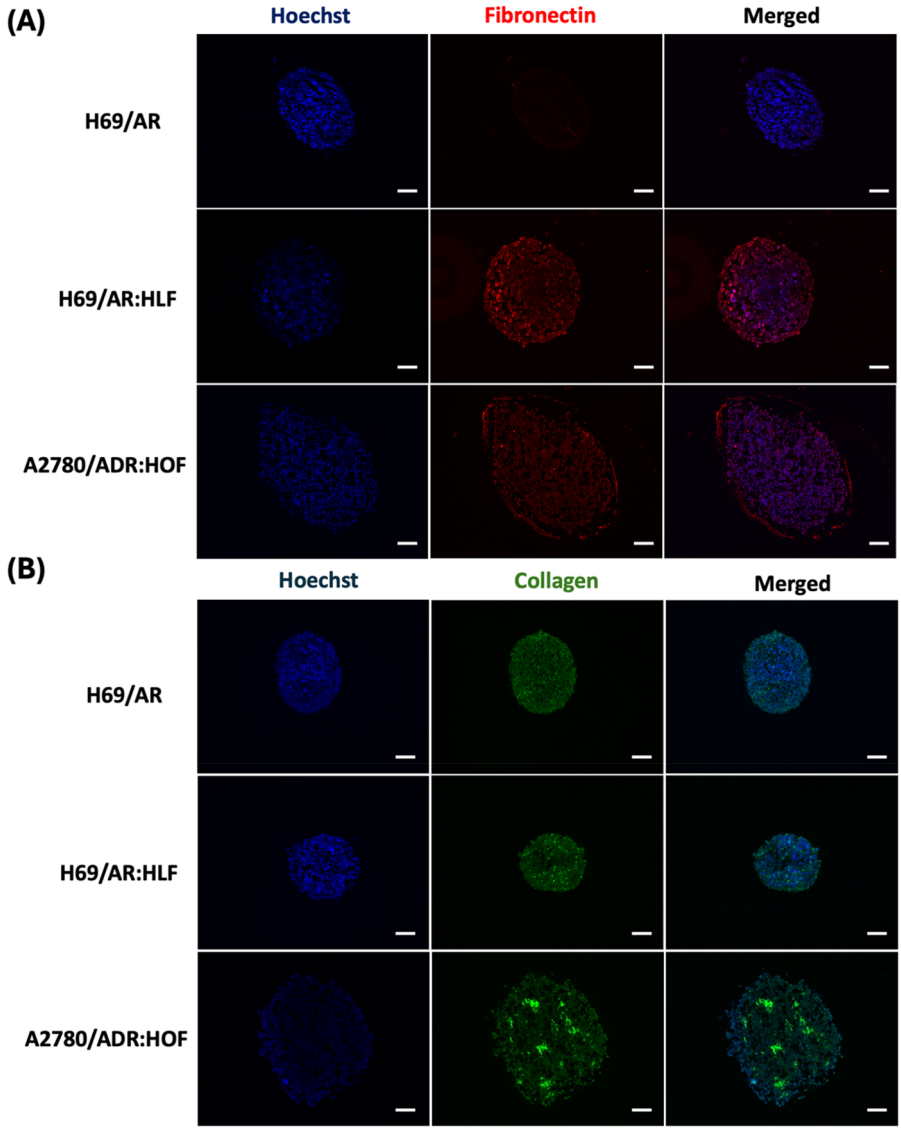


Figure 2. Characterization of spheroid ECM. Representative epifluorescence micrographs of sectioned H69/AR monoculture, H69/AR:HLF co-culture and A278/AD:HOF co-culture spheroids stained with Hoechst nuclear stain and immunostained to visualize (A) fibronectin and (B) collagen. Scale bars represent 100 µm.

shows that the integral green fluorescence to OD ratio was significantly lower in 5-day old co-culture spheroids compared to 3-day old co-culture spheroids ($p < 0.01$, Student's *t*-test). Figure 4(D) also shows that the 5-day old triple co-culture spheroids had a similar integral green fluorescence to OD ratio as the 5-day old co-culture spheroids and their integral red fluorescence to OD ratio was significantly lower than their integral green fluorescence to OD ratio ($p < 0.01$, Student's *t*-test).

### *Cytotoxic effect of STPP liposomes*

The STPP liposomes (4 mol% STPP in 5 mg/mL total lipid) used had a particle size of 112 ± 1 nm, a PDI of 0.29 ± 0.01 and a zeta potential of −7 ± 1 mV. The cytotoxicity of STPP liposomes was assessed using the CellTiter 96® Aqueous one solution cell proliferation assay for monolayer cell cultures and the CellTiter-Glo® 3D assay for spheroid cultures. Figure 5(A) shows that treatment with STPP liposomes at a concentration of 80 µM resulted in complete cell death within 24 h in monolayer cultures of H69/AR, HLF, and HUVEC cells. However, when the liposomes were tested on spheroids, the results revealed a different toxicity profile. Figure 5(B) shows that in H69/AR monoculture, co-culture, and triple co-culture spheroids exposed to 80 µM STPP liposomes, cell viability remained around 80% after 24 h while at 48 h, cell viability was significantly lower in monoculture spheroids than in co-culture or triple co-culture spheroids ($p < 0.01$, two-way ANOVA, Tukey's multiple comparison *post hoc* test). Figure 5(C) shows that STPP liposomes at an 80 µM concentration resulted in complete cell death in A2780/ADR, HOF, and HUVEC monolayer cultures within 24 h. Figure 5(D) shows that after exposure to 80 µM STPP liposomes, A2780/ADR co-culture and triple co-culture spheroids showed approximately 80% cell viability after 24 h while after 48 h, cell viability was significantly lower in triple co-culture spheroids compared to co-culture spheroids ($p < 0.01$, two-way ANOVA, Tukey's multiple comparison *post hoc* test).

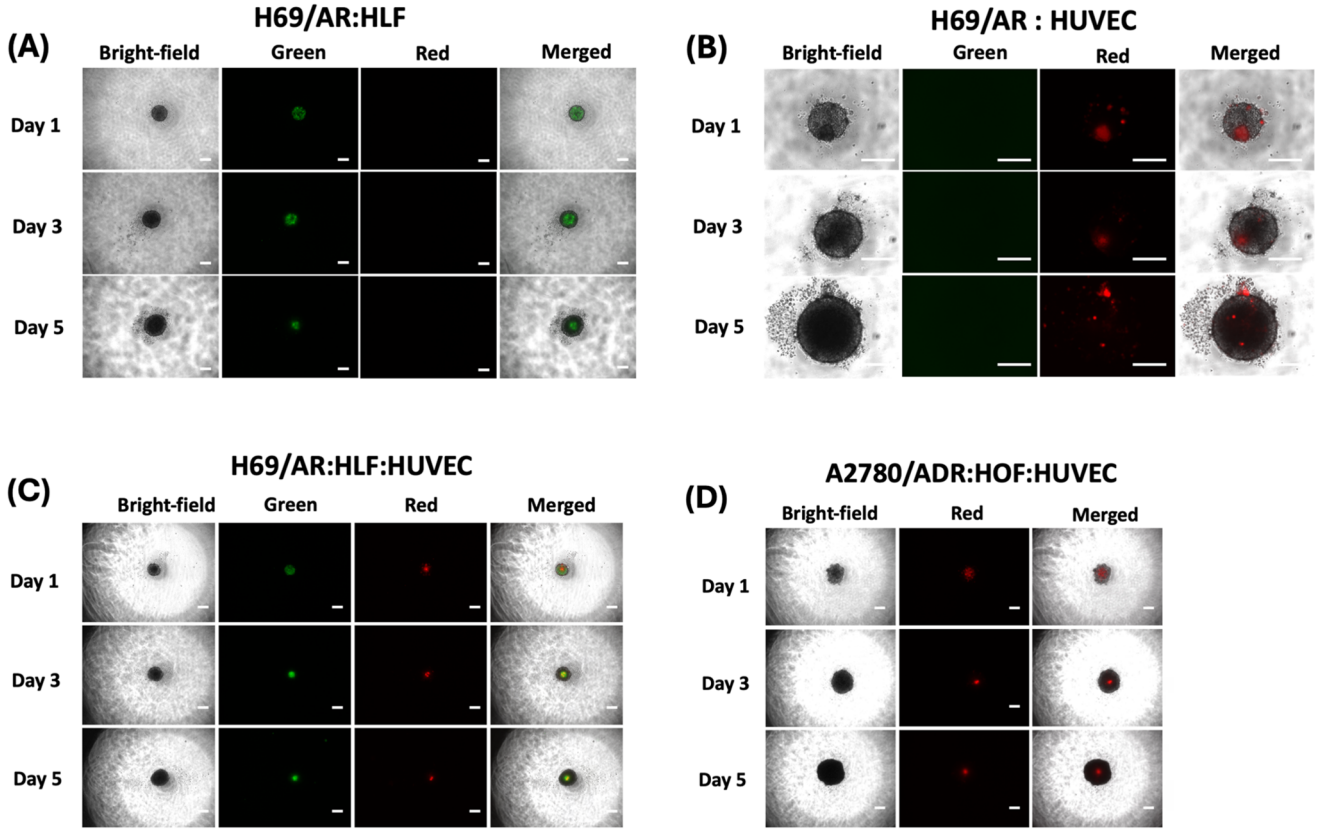


Figure 3. Characterization of spheroid cell composition. Representative epifluorescence micrographs of (A) H69/AR:HLF co-culture, (B) H69/AR:HUVEC co-culture, (C) H69/AR:HLF:HUVEC triple co-culture (D) and A2780/ADR:HOF:HUVEC triple co-culture spheroids. Green and red channels show GFP expressing HLF and RFP expressing HUVEC respectively. Scale bars represent 250 µm. Micrographs in panels A, C and D are at 1x magnification, those in panel B are at 3× magnification.

## Discussion

The development of more physiologically relevant and predictive *in vitro* models for cancer research remains a crucial challenge, especially in drug testing and therapeutic development [40,41]. While monolayer cultures are widely used, their limitations in mimicking the intricate architecture and microenvironment of *in vivo* tumors are well-documented [9,42,43]. These conventional models do not accurately represent the three-dimensional interactions between cells and their extracellular matrix (ECM), leading to significant discrepancies in the assessment of drug efficacy and toxicity [44–49]. This gap in modeling likely contributes to a low translational success rate from preclinical studies to clinical applications. In this context, spheroids have emerged as a potentially superior alternative to monolayer cultures [45,50]. Since their introduction in the 1970s, monoculture tumor spheroids—composed solely of cancer cells have been used to provide insights into cancer cell interactions, proliferation, and therapeutic responses [13,14]. However, tumors are not composed of cancer cells alone but include other cell types like fibroblasts, endothelial cells, and immune cells that all play a role in developing the tumor microenvironment (TME) [18,19,51]. Therefore, incorporating some of these cell types cells in addition to tumor cells within the spheroid is a logical next step in the development of spheroid models that more closely mimic the *in vivo* TME. However, efforts to integrate non-tumor cell types into these models have been relatively limited. This limitation largely stems from the complex culture and characterization procedures required to maintain a balanced interaction between multiple cell types. Not all tumor cells readily form spheroids. For tumor cells that can form spheroids, differences in growth rates, cell signaling, and extracellular matrix interactions between tumor and non-tumor cells can often present practical challenges. Nevertheless, the ethical and financial burden of animal models, along with a stronger commitment to the 3Rs principles—Replacement, Reduction, and Refinement—have driven a renewed interest in improving *in vitro* tumor models [52,53].

While multicellular spheroids of colorectal and pancreatic ductal adenocarcinomas incorporating three cell types, have been previously reported, the fibroblasts used in these were often of lung origin, which might not accurately represent the stromal interactions occurring in these tumors [54,55]. Therefore, the inclusion of tissue-specific fibroblasts was prioritized for the spheroid models tested in this study. Drug resistant lung and ovarian carcinomas were chosen as the models for development. Lung cancer is the leading cause of cancer-related mortality worldwide, characterized by a complex TME predominantly composed of tumor cells and fibroblasts [56,57]. This intricate TME plays a critical role in driving tumor progression and resistance to therapeutic interventions [57]. Ovarian cancer, while less common, is associated with late diagnosis and poor prognosis, largely due to a protective TME that supports tumor survival and metastasis [56,58]. In addition, ovarian cancer exhibits a distinctive mode

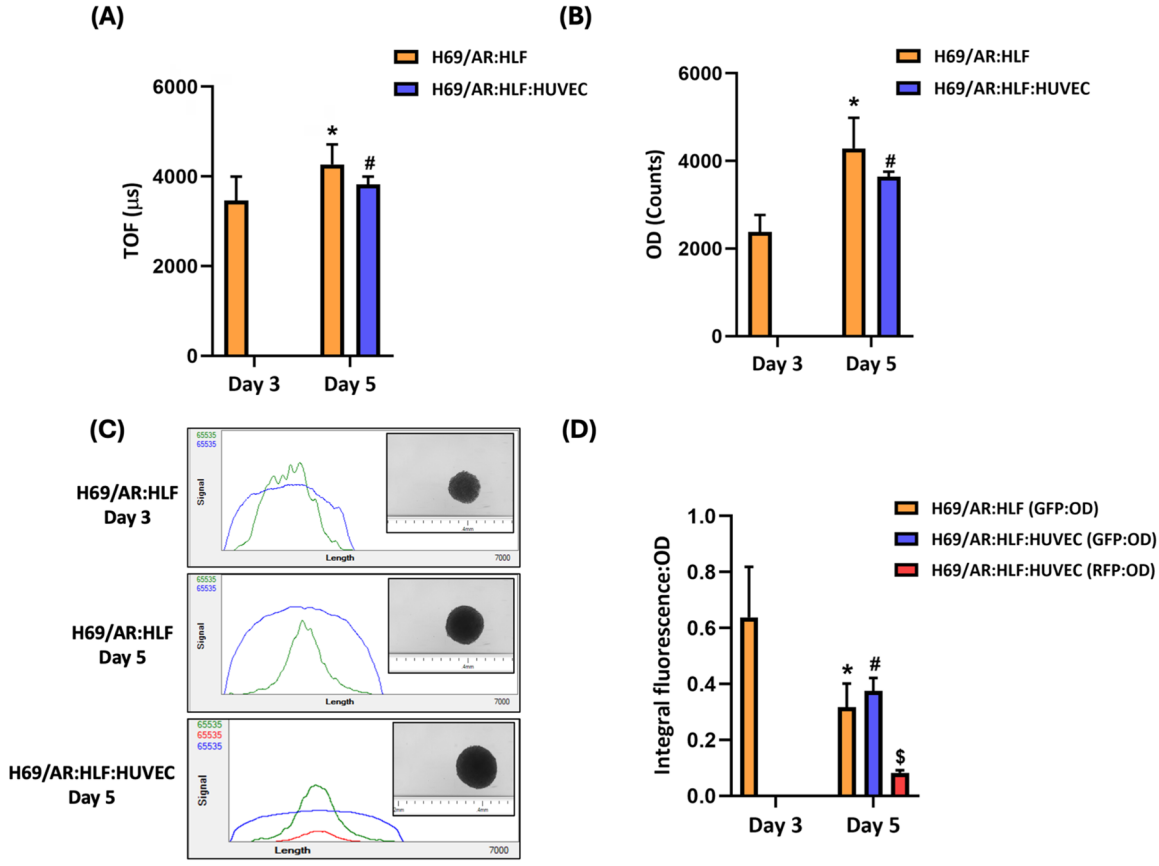


Figure 4. Characterization of spheroid architecture. Large particle flow cytometer measurements of (A) Time of flight (TOF) of 3 and 5 day old H69/AR:HLF co-culture and 5 day old H69/AR:HLF:HUVEC triple co-culture spheroids; (B) Optical density (OD) of 3 and 5 day old H69/AR:HLF co-culture and 5-day old H69/AR:HLF:HUVEC triple co-culture spheroids. (C) Representative profiler plots of signal intensity across individual spheroids optical density (blue), green fluorescence (green), and red fluorescence (red) for each plot for 3 and 5 day old H69/AR:HLF co-culture and 5 day old H69/AR:HLF:HUVEC triple co-culture spheroids. GFP and RFP expressing variants of HLF and HUVEC respectively were used. For each plot, inset shows corresponding monochrome image of the spheroid analyzed. (D) Integral fluorescence to OD signal ratios for green fluorescence (GFP:OD) in 3-and 5-day old H69/AR:HLF co-culture and 5-day H69/AR:HLF:HUVEC triple co-culture; red fluorescence (RFP:OD) for 5-day old triple co-culture spheroids. Data are mean ± standard deviation ($n > 200$). Student *t*-test *$p < 0.01$ vs. 3 day H69/AR:HLF, #$p < 0.01$ vs. 5 day H69/AR:HLF spheroid, \$$p < 0.01$ vs. 5 day H69/AR:HLF:HUVEC spheroid.

of metastatic spread, wherein tumor cells are shed into the peritoneal cavity and form spheroid-like aggregates within ascetic fluid [59]. These aggregates remain viable in suspension, interact with stromal and immune cells, and subsequently adhere to distant mesothelial surfaces, leading to widespread peritoneal colonization [60–62]. This non-hematogenous dissemination pathway, together with a permissive stromal niche, contributes to the rapid disease progression and high relapse rates observed in ovarian cancer [62].

Three types of spheroids were developed for each tumor type in this study: monoculture spheroids composed solely of drug-resistant tumor cells, co-culture spheroids composed of drug resistant-tumor cells and tissue specific fibroblasts, and triple co-culture spheroids composed of drug-resistant tumor cells, fibroblasts, and endothelial cells. While H69/AR cells readily formed monoculture spheroids, A2780/ADR cells consistently failed to form monoculture spheroids under identical conditions. However, when co-cultured with HOF, the A2780/ADR cells easily formed spheroids (Figure 1). This finding highlights fundamental biological differences between the two cancer cell lines, potentially related to cell adhesion properties, dependence on extracellular matrix (ECM) components, or specific growth factor requirements. These elements provide structural and biochemical support for cell aggregation, survival, and tumor progression *in vivo* and are absent *in vitro* especially in monocultures. Further support for this concept is provided by the patterns of fibronectin and collagen staining seen Figure 2. Fibronectin, a critical ECM glycoprotein, is known to regulate tumor cell adhesion, migration, and survival by interacting with integrins and other cell surface receptors [63,64]. This interaction plays a pivotal role in enhancing the metastatic potential of tumor cells by facilitating dynamic changes in the TME [63–65]. Collagen serves as a fundamental structural component of the ECM, contributing to the mechanical properties of tissues, such as stiffness, which can act as both a scaffold for cells and a physical barrier to therapeutic agents, potentially reducing drug penetration and efficacy [66]. Figure 2(A) shows that fibronectin staining was much lower H69/AR monoculture spheroids than in H69/AR co-culture spheroids. This suggests that fibroblasts play a crucial role in contributing to a more complex tumor-like ECM in the spheroid. Fibronectin is known to promote cell adhesion and aggregation which are critical steps in spheroid formation [67]. The high level of fibronectin staining observed in A2780/ADR co-culture spheroids also suggests that fibroblast-driven ECM production might be the critical factor to stimulate the development of A2780/ADR

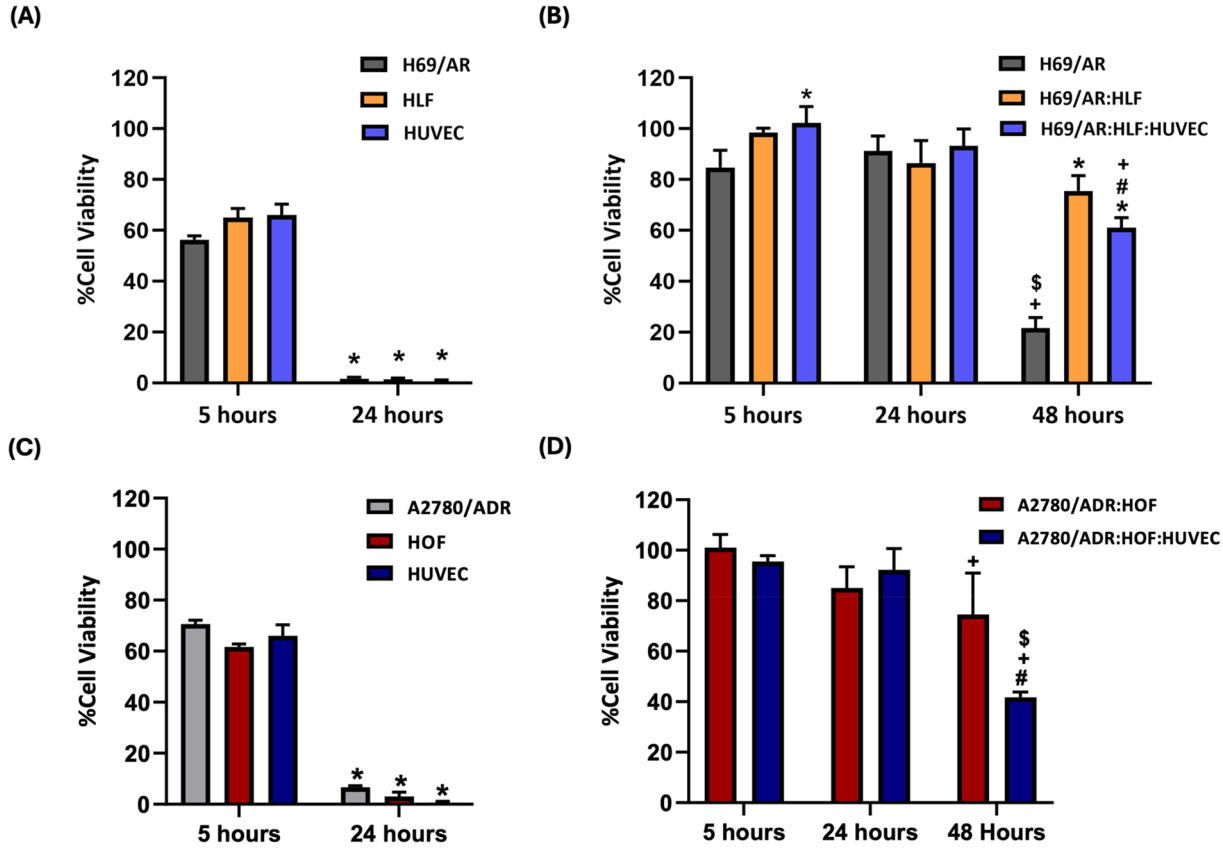


Figure 5. Characterization of STPP liposome toxicity. Measurement of cell viability after exposure for indicated times to STPP liposomes at a concentration of 80 µM in (A) H69/AR, HLF, and HUVEC monolayer cultures, (B) H69/AR monoculture, H69/AR:HLF co-culture and H69/AR:HLF:HUVEC triple co-culture spheroids, (C) A2780/ADR, HOF, and HUVEC monolayer cultures, (D) A2780/ADR:HOF co-culture and A2780/ADR:HOF:HUVEC triple co-culture spheroids. Data are mean ± standard deviation ($n = 4$). For monolayer cultures: Student's *t*-test. *$p < 0.01$ vs. corresponding groups at 5 h. For spheroid cultures-two-way ANOVA, followed by Tukey's multiple comparison *post hoc* test. *$p < 0.01$ vs. H69/AR spheroid, #$p < 0.01$ vs. H69/AR:HLF or A2780/ADR:HOF within corresponding time intervals. +$p < 0.01$ vs. 5 h, \$$p < 0.01$ vs. 24 h within respective groups for both lung and ovarian tumor spheroids.

spheroids. Collagen was present in both H69/AR monoculture and co-culture spheroids as well as in A2780/ADR co-culture spheroids (Figure 2(B)). These findings align with the well-established role of collagen as an universal ECM component that influences the biophysical properties of the tumor microenvironment across different cancer types [66]. Collagen is known to play a role in increasing tissue stiffness, which is particularly relevant in the context of tumor progression. A stiffer ECM can promote cancer cell invasiveness and may also limit drug penetration, thereby contributing to therapeutic resistance. Taken together these observations demonstrate the role fibroblasts can play in providing essential biochemical support to facilitate spheroid formation and generation of an ECM composition *in vitro* which more closely mimics that of *in vivo* solid tumors. When human umbilical vein endothelial cells (HUVECs) were introduced alongside tumor cells and fibroblasts, triple co-culture spheroids were readily formed by both H69/AR and A2780/ADR cells. Notably, A2780/ADR cells co-cultured with HOF and HUVECs formed compact spheroids as early as day 1. In contrast, looser aggregates were initially observed in the A2780/ADR:HOF co-culture and compact spheroid formation then occurred gradually over time. Endothelial cells are known to secrete ECM components and growth factors that facilitate tighter cellular organization by promoting adhesion and communication between tumor and stromal cells [68–71]. The formation of compact spheroids in the A2780/ADR-HOF-HUVEC triple co-culture suggests that HUVECs can accelerate the development of a stable three-dimensional structure, potentially by reinforcing the structural framework of the spheroid through their interactions with fibroblasts and tumor cells.

The next step in the study involved analyzing the growth characteristics of the developed monoculture, co-culture, and triple co-culture spheroids. The H69/AR monoculture spheroids exhibited a significantly larger diameter compared to the co-culture and triple co-culture spheroids (Figure 1(C)). This was consistent with their higher ATP concentrations across all time points measured (Figure 1(E)). Interestingly, the diameters and ATP concentrations of H69/AR co-culture and triple co-culture spheroids were similar. In the case of A2780/ADR co-culture and triple co-culture spheroids, initial observations revealed loose aggregates that gradually compacted over time. Although their diameters remained relatively unchanged during early formation, the ATP concentration increased significantly as the culture progressed, indicating an increase metabolic activity (Figure 1(D,F)). The increase in metabolic activity suggests that while the initial spheroid structure may not have expanded substantially, there is continued cell proliferation within the spheroid.

In order to confirm the presence of each cell type and their distribution within the co-culture and triple co-culture

spheroids it was essential to use cells that had been constitutively labeled with a fluorescent marker. Cell lines genetically modified to express fluorescent protein are the most convenient and reliable way of tracking multiple cell types in mixed cultures. HLF and HUVEC variants expressing green fluorescent protein and red fluorescent protein respectively are commercially available and when co-cultured with H69/AR tumor cells can be easily identified by their fluorescence emissions. Unfortunately, a suitable fluorescent protein expressing variant of the HOF cell line was not commercially available precluding a similar analysis of A2780/ADR co-culture and triple co-culture spheroids. Epifluorescence micrographs of H69/AR:HLF co-culture and H69/AR:HUVEC co-culture spheroids in Figure 3 show that both HLFs and HUVECs were not homogenously distributed but had distinct location preferences within the spheroid mass. Interestingly, the location of HUVECs changed with the presence of fibroblasts in the triple co-culture spheroid. Rather than being distributed toward the periphery of the spheroid, the HUVECs in the triple co-culture spheroid appeared co-located with the HLFs in the central region of the spheroid mass. In the A2780/ADR:HOF:HUVEC triple co-culture with RFP expressing HUVECs, the HUVEC fluorescence was localized in the central region of the spheroid mass as well. Taken together these qualitative data suggest that there are cell specific dynamic interactions occurring in the co-culture and triple co-culture spheroids that are likely similar to those in the *in vivo* TME.

Large-particle flow cytometry was utilized to further analyze the cellular composition and distribution within the spheroids. This technique can analyze a large number of spheroids and provide information on physical dimensions of the spheroids as well as spatial distribution of cell populations within the spheroid structures. TOF and opacity measurements shown in Figure 4(A,B), respectively confirmed that both H69/AR co-culture and triple co-culture spheroids increased in size and density over time, consistent with microscopic analysis. Cellular localization within the spheroids was assessed by capturing forward scatter to identify the overall structure, green fluorescence to detect HLF cells, and red fluorescence to detect HUVECs. Figure 4(C) shows that on day 3, the green fluorescence signal corresponding to HLFs was distributed across the co-culture spheroids, but by day 5, a significant shift was observed, with the green fluorescence becoming concentrated toward the center of the spheroids as was previously seen by microscopy. This redistribution of cells could be because H69/AR cells proliferated more rapidly than HLFs and confined the HLFs within the center of the spheroid. However, given that HLF and H69/AR cells exhibited similar growth rates when cultured in flasks a more likely explanation is that HLFs actively migrated toward the core of the spheroid. As the spheroids increased in size, nutrient and oxygen diffusion likely became limited, particularly in the central regions, creating a hypoxic environment. Fibroblasts are known to migrate toward hypoxic regions where they engage in ECM remodeling and support tissue repair processes [72–74]. The dynamic redistribution of HLFs shows how the incorporation of stromal cells can enable spheroids to more closely mimic tissue remodeling processes that are known to occur during tumor progression *in vivo*.

In triple co-culture spheroids, the green fluorescence signal of HLFs, was concentrated in the center, similar to the pattern observed on day 5 in the co-culture spheroids. As previously observed by microscopy, the red fluorescence of HUVECs was also concentrated in the central region of the triple co-culture spheroids. Endothelial cells typically localize in oxygen- and nutrient-rich regions *in vivo*, and would be expected to be found at the periphery of the spheroids as was observed by microscopy in H69/AR:HUVEC co-culture spheroids. However, fibroblasts are known to produce ECM components such as collagen and fibronectin, which remodel the microenvironment and influence cellular interactions. Moreover, fibroblasts secrete pro-angiogenic factors such as VEGF, which may attract endothelial cells [75]. In this context, the presence of HLFs sufficiently altered the ECM structure resulting in the localization of HUVECs within the spheroid core. In contrast, when HLFs were absent, the ECM was less structured, and tumor-endothelial interactions were less organized, leading to peripheral localization of HUVECs, where oxygen and nutrient availability are higher [76]. Collectively, These findings indicate that fibroblasts play a crucial role in modulating the behavior and spatial organization of endothelial cells within tumor spheroids.

After characterization of the spheroids, their potential as a more discriminating *in vitro* model was tested using a treatment with a previously demonstrated effect. Liposomes modified with stearyl triphenyl phosphonium (STPP) have been shown to have a higher toxicity in drug resistant lung and ovarian tumor cell lines compared to nonresistant cell lines [38]. The observed effect is unique to STPP incorporated in liposomes and is most likely mediated by STPP induced uncoupling of oxidative phosphorylation that has been reported to be upregulated in drug resistant tumor cells [38]. The dose at which the selective toxicity is observed is too high to warrant further investigation in *in vivo* models but STPP liposomes are still a convenient test treatment for evaluation in the spheroid models developed in this study. To establish a baseline, individual cell types used in spheroid formation were first exposed to STPP in monolayer cultures for 5 and 24 h. In all cases, STPP liposomes resulted in complete cell death in the monolayers, confirming their previously reported cytotoxicity on monolayer cultures. Spheroids formed from both H69/AR and A2780/ADR cells were then treated with STPP liposomes for 5, 24, and 48 h. STPP liposomes failed to induce significant toxicity in monoculture spheroids at 24 h. Co-culture spheroids containing fibroblasts as well as triple co-culture spheroids with fibroblasts and endothelial cells, exhibited minimal toxicity after 48 h of treatment (Figure 5). These findings offer two critical insights: first, the cytotoxic profile of STPP liposomes differs markedly between monolayer and spheroid models. Second, the inclusion of stromal components such as fibroblasts and endothelial cells significantly alters the response to STPP liposomes. Collectively these findings suggest the value of using spheroid models for more discriminating *in vitro* assessments of therapeutic efficacy and the importance of incorporating multiple cell types in spheroid models to more closely replicate the characteristics of the *in vivo* TME. Moreover, spheroids of this type can be economically produced in large

numbers to afford the testing of a large number of formulation and dosing combinations to optimize antitumor treatments prior to testing in *in vivo* models. Liposomal formulation optimization studies in particular can greatly benefit from such testing to develop optimal lipid composition and drug loading to maximize antitumor effect.

## Conclusion

Multicellular spheroids incorporating fibroblasts and endothelial cells, in addition to tumor cells, exhibited several key characteristics that closely mimic the *in vivo* TME. Notably, the inclusion of non-tumor stromal cells led to increased expression of fibronectin, indicating active ECM remodeling within the model. As the spheroids grew in size, fibroblasts demonstrated directional migration toward the spheroid core—a behavior consistent with stromal dynamics observed in solid tumors. Additionally, HUVECs preferentially localized to fibroblast-rich regions, reflecting structural and spatial characteristics commonly seen in native tumor tissues. These findings underscore the enhanced physiological relevance of our co-culture spheroids for evaluating experimental tumor therapies *in vitro* prior to *in vivo* validation. Moving forward, future studies can build upon this work by incorporating additional components of the tumor microenvironment, such as immune cells (e.g. macrophages, T cells) or adipocytes, to further enhance the physiological relevance of these models. Integration of flow-based systems or microfluidic platforms can help simulate interstitial fluid dynamics and drug transport more realistically, offering a more comprehensive assessment of therapeutic distribution and response. Additionally, leveraging advanced imaging techniques and single-cell resolution analyses may provide deeper insight into spatial drug penetration, cellular heterogeneity, and localized treatment responses within these complex spheroids. These enhancements would not only improve the predictive accuracy of *in vitro* platforms but also support their use as ethically and economically viable alternatives to in vivo testing in early-phase drug development.

## Acknowledgements

The authors wish to acknowledge Madelyn Davis and Julia Thompson from Union Biometrica, Inc. for their assistance with studies conducted using the large particle flow cytometer.

## Author contributors

**Shrey Shah:** Investigation, Methodology, Validation, Formal analysis, Writing original draft, Visualization, Funding acquisition. **Yongwoon Kim:** Investigation, Methodology, Validation. **Rock Pulak**: Methodology, Supervision, Resources. **Gerard G.M. D'Souza:** Conceptualization, Visualization, Supervision, Project administration, Funding acquisition, Writing- Review & Editing.

## Disclosure statement

No potential conflict of interest was reported by the author(s).

## Funding

This work was supported by funding from the MCPHS University School of Pharmacy-Boston, the MCPHS University Center for Research and Discovery and Massachusetts Life Sciences Center Capital Grants to MCPHS University.

## References

[1] Wang L, Hu D, Xu J, et al. Complex *in vitro* model: a transformative model in drug development and precision medicine. Clin Transl Sci. 2023;17(2). doi: 10.1111/cts.13695.
[2] Wilding JL, Bodmer WF. Cancer cell lines for drug discovery and development. Cancer Res. 2014;74(9):2377–2384. doi: 10.1158/0008-5472.CAN-13-2971.
[3] Jubelin C, Muñoz-Garcia J, Griscom L, et al. Three-dimensional *in vitro* culture models in oncology research. Cell Biosci. 2022;12(1):155. doi: 10.1186/s13578-022-00887-3.
[4] Karlsson H, Fryknäs M, Larsson R, et al. Loss of cancer drug activity in colon cancer HCT-116 cells during spheroid formation in a new 3-D spheroid cell culture system. Exp Cell Res. 2012;318(13):1577–1585. doi: 10.1016/j.yexcr.2012.03.026.
[5] Barbosa MAG, Xavier CPR, Pereira RF, et al. 3D cell culture models as recapitulators of the tumor microenvironment for the screening of anti-cancer drugs. Cancers. 2021;14(1):190. doi: 10.3390/cancers14010190.
[6] Lv D, Hu Z, Lu L, et al. Three-dimensional cell culture: a powerful tool in tumor research and drug discovery. Oncol Lett. 2017;14(6):6999–7010. doi: 10.3892/ol.2017.7134.
[7] Breslin S, O'Driscoll L. Three-dimensional cell culture: the missing link in drug discovery. Drug Discov Today. 2013;18(5–6):240–249. doi: 10.1016/j.drudis.2012.10.003.
[8] Zanoni M, Piccinini F, Arienti C, et al. 3D tumor spheroid models for in vitro therapeutic screening: a systematic approach to enhance the biological relevance of data obtained. Sci Rep. 2016;6(1):19103. doi: 10.1038/srep19103.
[9] Benien P, Swami A. 3D tumor models: history, advances and future perspectives. Future Oncol. 2014;10(7):1311–1327. doi: 10.2217/fon.13.274.
[10] Langan LM, Dodd NJF, Owen SF, et al. Direct measurements of oxygen gradients in spheroid culture system using electron parametric resonance oximetry. PLOS One. 2016;11(2):e0149492. doi: 10.1371/journal.pone.0149492.
[11] Mehta G, Hsiao AY, Ingram M, et al. Opportunities and challenges for use of tumor spheroids as models to test drug delivery and efficacy. J Control Release. 2012;164(2):192–204. doi: 10.1016/j.jconrel.2012.04.045.
[12] Sutherland RM, McCredie JA, Inch WR. Growth of multicell spheroids in tissue culture as a model of nodular carcinomas. J Natl Cancer Inst. 1971;46(1):113–120.
[13] Weiswald L-B, Richon S, Validire P, et al. Newly characterised *ex vivo* colospheres as a three-dimensional colon cancer cell model of tumour aggressiveness. Br J Cancer. 2009;101(3):473–482. doi: 10.1038/sj.bjc.6605173.
[14] Mitrakas AG, Tsolou A, Didaskalou S, et al. Applications and advances of multicellular tumor spheroids: challenges in their development and analysis. Int J Mol Sci. 2023;24(8):6949. doi: 10.3390/ijms24086949.
[15] Erlanson M, Daniel-Szolgay E, Carlsson J. Relations between the penetration, binding and average concentration of cytostatic drugs in human tumour spheroids. Cancer Chemother Pharmacol. 1992;29(5):343–353. doi: 10.1007/BF00686002.
[16] Perche F, Patel NR, Torchilin VP. Accumulation and toxicity of antibody-targeted doxorubicin-loaded PEG-PE micelles in ovarian cancer cell spheroid model. J Control Release. 2012;164(1):95–102. doi: 10.1016/j.jconrel.2012.09.003.

[17] Solomon MA, Lemera J, D'Souza GG. Development of an in vitro tumor spheroid culture model amenable to high-throughput testing of potential anticancer nanotherapeutics. J Liposome Res. 2016;26(3):246–260. doi: 10.3109/08982104.2015.1105820.
[18] Anderson NM, Simon MC. The tumor microenvironment. Curr Biol. 2020;30(16):R921–R925. doi: 10.1016/j.cub.2020.06.081.
[19] Baghban R, Roshangar L, Jahanban-Esfahlan R, et al. Tumor microenvironment complexity and therapeutic implications at a glance. Cell Commun Signal. 2020;18(1):59. doi: 10.1186/s12964-020-0530-4.
[20] Werb Z, Lu P. The role of stroma in tumor development. Cancer J. 2015;21(4):250–253. doi: 10.1097/PPO.0000000000000127.
[21] Xing F, Saidou J, Watabe K. Cancer associated fibroblasts (CAFs) in tumor microenvironment. Front Biosci. 2010;15(1):166–179. doi: 10.2741/3613.
[22] Fotsitzoudis C, Koulouridi A, Messaritakis I, et al. Cancer-associated fibroblasts: the origin, biological characteristics and role in cancer-a glance on colorectal cancer. Cancers. 2022;14(18):4394.), doi: 10.3390/cancers14184394.
[23] Min A, Zhu C, Wang J, et al. Focal adhesion kinase knockdown in carcinoma-associated fibroblasts inhibits oral squamous cell carcinoma metastasis via downregulating MCP-1/CCL2 expression. J Biochem Mol Toxicol. 2015;29(2):70–76. doi: 10.1002/jbt.21669.
[24] Liu J, Chen S, Wang W, et al. Cancer-associated fibroblasts promote hepatocellular carcinoma metastasis through chemokine-activated hedgehog and TGF-beta pathways. Cancer Lett. 2016;379(1):49–59. doi: 10.1016/j.canlet.2016.05.022.
[25] Jobe NP, Rösel D, Dvořánková B, et al. Simultaneous blocking of IL-6 and IL-8 is sufficient to fully inhibit CAF-induced human melanoma cell invasiveness. Histochem Cell Biol. 2016;146(2):205–217. doi: 10.1007/s00418-016-1433-8.
[26] Belhabib I, Zaghdoudi S, Lac C, et al. Extracellular matrices and cancer-associated fibroblasts: targets for cancer diagnosis and therapy? Cancers. 2021;13(14):3466. doi: 10.3390/cancers13143466.
[27] Popova NV, Jücker M. The functional role of extracellular matrix proteins in cancer. Cancers. 2022;14(1):238. doi: 10.3390/cancers14010238.
[28] Erdogan B, Ao M, White LM, et al. Cancer-associated fibroblasts promote directional cancer cell migration by aligning fibronectin. J Cell Biol. 2017;216(11):3799–3816. doi: 10.1083/jcb.201704053.
[29] Masi I, Ottavi F, Caprara V, et al. The extracellular matrix protein type I collagen and fibronectin are regulated by β-arrestin-1/endothelin axis in human ovarian fibroblasts. J Exp Clin Cancer Res. 2025;44(1):64. doi: 10.1186/s13046-025-03327-5.
[30] Jiang X, Wang J, Deng X, et al. The role of microenvironment in tumor angiogenesis. J Exp Clin Cancer Res. 2020;39(1):204. doi: 10.1186/s13046-020-01709-5.
[31] Coursier D, Calvo F. CAFs vs. TECs: when blood feuds fuel cancer progression, dissemination and therapeutic resistance. Cell Oncol. 2024;47(4):1091–1112. doi: 10.1007/s13402-024-00931-z.
[32] Huang B, Huang M, Li Q. Cancer-associated fibroblasts promote angiogenesis of hepatocellular carcinoma by VEGF-mediated EZH2/VASH1 pathway. Technol Cancer Res Treat. 2019;18:1533033819879905. doi: 10.1177/1533033819879905.
[33] Feng Y, Luo S, Fan D, et al. The role of vascular endothelial cells in tumor metastasis. Acta Histochem. 2023;125(6):152070. doi: 10.1016/j.acthis.2023.152070.
[34] Maishi N, Ohba Y, Akiyama K, et al. Tumour endothelial cells in high metastatic tumours promote metastasis via epigenetic dysregulation of biglycan. Sci Rep. 2016;6(1):28039. doi: 10.1038/srep28039.
[35] Zhao R, Bei X, Yang B, et al. Endothelial cells promote metastasis of prostate cancer by enhancing autophagy. J Exp Clin Cancer Res. 2018;37(1):221. doi: 10.1186/s13046-018-0884-2.
[36] Fang J, Lu Y, Zheng J, et al. Exploring the crosstalk between endothelial cells, immune cells, and immune checkpoints in the tumor microenvironment: new insights and therapeutic implications. Cell Death Dis. 2023;14(9):586. doi: 10.1038/s41419-023-06119-x.
[37] Xu Y, Miller CP, Tykodi SS, et al. Signaling crosstalk between tumor endothelial cells and immune cells in the microenvironment of solid tumors. Front Cell Dev Biol. 2024;12:1387198. doi: 10.3389/fcell.2024.1387198.
[38] Shah S, Ouellette M, D'Souza GGM. In vitro assessment of stearyl triphenyl phosphonium toxicity in drug-resistant tumor cells. 4open. 2022;5:6. doi: 10.1051/fopen/2022003.
[39] Solomon MA, Shah AA, D'Souza GG. In vitro assessment of the utility of stearyl triphenyl phosphonium modified liposomes in overcoming the resistance of ovarian carcinoma ovcar-3 cells to paclitaxel. Mitochondrion. 2013;13(5):464–472. doi: 10.1016/j.mito.2012.10.013.
[40] Johnson A, Reimer S, Childres R, et al. The applications and challenges of the development of In vitro tumor microenvironment chips. Cell Mol Bioeng. 2023;16(1):3–21. doi: 10.1007/s12195-022-00755-7.
[41] Sharma K, et al. A comprehensive review of 3D cancer models for drug screening and translational research. Cancer Innov. 2024;3(1):e102.
[42] Pampaloni F, Reynaud EG, Stelzer EH. The third dimension bridges the gap between cell culture and live tissue. Nat Rev Mol Cell Biol. 2007;8(10):839–845. doi: 10.1038/nrm2236.
[43] Shah S, D'Souza GGM. Modeling tumor microenvironment complexity *in vitro*: Spheroids as physiologically relevant tumor models and strategies for their analysis. Cells. 2025;14(10):732. doi: 10.3390/cells14100732.
[44] Baker BM, Chen CS. Deconstructing the third dimension: how 3D culture microenvironments alter cellular cues. J Cell Sci. 2012;125(Pt 13):3015–3024. doi: 10.1242/jcs.079509.
[45] Kapalczynska M, et al. 2D and 3D cell cultures – a comparison of different types of cancer cell cultures. Arch Med Sci. 2018;14(4):910–919.
[46] Abbas ZN, Al-Saffar AZ, Jasim SM, et al. Comparative analysis between 2D and 3D colorectal cancer culture models for insights into cellular morphological and transcriptomic variations. Sci Rep. 2023;13(1):18380. doi: 10.1038/s41598-023-45144-w.
[47] Bennett LE, Edwards EB, Hosenpud JD. Transplantation with older donor hearts for presumed "stable" recipients: an analysis of the joint international society for heart and lung transplantation/united network for organ sharing thoracic registry. J Heart Lung Transplant. 1998;17(9):901–905.
[48] Verloy R, Privat-Maldonado A, Van Audenaerde J, et al. Capturing the heterogeneity of the PDAC tumor microenvironment: novel triple co-culture spheroids for drug screening and angiogenic evaluation. Cells. 2025;14(6):450. doi: 10.3390/cells14060450.
[49] Chong LH, Yip AK, Farm HJ, et al. The role of cell-matrix adhesion and cell migration in breast tumor growth and progression. Front Cell Dev Biol. 2024;12:1339251. doi: 10.3389/fcell.2024.1339251.
[50] Ong CS, Zhou X, Han J, et al. In vivo therapeutic applications of cell spheroids. Biotechnol Adv. 2018;36(2):494–505. doi: 10.1016/j.biotechadv.2018.02.003.
[51] Knipper K, Lyu SI, Quaas A, et al. Cancer-Associated fibroblast heterogeneity and its influence on the extracellular matrix and the tumor microenvironment. Int J Mol Sci. 2023;24(17):13482. doi: 10.3390/ijms241713482.
[52] Graham ML, Prescott MJ. The multifactorial role of the 3Rs in shifting the harm-benefit analysis in animal models of disease. Eur J Pharmacol. 2015;759:19–29. doi: 10.1016/j.ejphar.2015.03.040.
[53] Tannenbaum J, Bennett BT. Russell and burch's 3Rs then and now: the need for clarity in definition and purpose. J Am Assoc Lab Anim Sci. 2015;54(2):120–132.
[54] Lazzari G, Nicolas V, Matsusaki M, et al. Multicellular spheroid based on a triple co-culture: a novel 3D model to mimic pancreatic tumor complexity. Acta Biomater. 2018;78:296–307. doi: 10.1016/j.actbio.2018.08.008.
[55] Bauleth-Ramos T, Feijão T, Gonçalves A, et al. Colorectal cancer triple co-culture spheroid model to assess the biocompatibility and

anticancer properties of polymeric nanoparticles. J Control Release. 2020;323:398–411. doi: 10.1016/j.jconrel.2020.04.025.
[56] Sung H, Ferlay J, Siegel RL, et al. Global cancer statistics 2020: GLOBOCAN estimates of incidence and mortality worldwide for 36 cancers in 185 countries. CA Cancer J Clin. 2021;71(3):209–249. doi: 10.3322/caac.21660.
[57] Altorki NK, Markowitz GJ, Gao D, et al. The lung microenvironment: an important regulator of tumour growth and metastasis. Nat Rev Cancer. 2019;19(1):9–31. doi: 10.1038/s41568-018-0081-9.
[58] Yang Y, Yang Y, Yang J, et al. Tumor microenvironment in ovarian cancer: function and therapeutic strategy. Front Cell Dev Biol. 2020;8:758. doi: 10.3389/fcell.2020.00758.
[59] de la Fuente A, Alonso-Alconada L, Costa C, et al. M-Trap: exosome-based capture of tumor cells as a new technology in peritoneal metastasis. J Natl Cancer Inst. 2015;107(9):djv184. doi: 10.1093/jnci/djv184.
[60] Parashar D, Nair B, Geethadevi A, et al. Peritoneal spread of ovarian cancer harbors therapeutic vulnerabilities regulated by FOXM1 and EGFR/ERBB2 signaling. Cancer Res. 2020;80(24):5554–5568. doi: 10.1158/0008-5472.CAN-19-3717.
[61] Rickard BP, Conrad C, Sorrin AJ, et al. Malignant ascites in ovarian cancer: cellular, acellular, and biophysical determinants of molecular characteristics and therapy response. Cancers. 2021;13(17):4318. doi: 10.3390/cancers13174318.
[62] Boylan KLM, Manion RD, Shah H, et al. Inhibition of ovarian cancer cell spheroid formation by synthetic peptides derived from nectin-4. Int J Mol Sci. 2020;21(13):4637. doi: 10.3390/ijms21134637.
[63] Spada S, Tocci A, Di Modugno F, et al. Fibronectin as a multiregulatory molecule crucial in tumor matrisome: from structural and functional features to clinical practice in oncology. J Exp Clin Cancer Res. 2021;40(1):102. doi: 10.1186/s13046-021-01908-8.
[64] Li J, Chen C, Chen B, et al. High FN1 expression correlates with gastric cancer progression. Pathol Res Pract. 2022;239:154179. doi: 10.1016/j.prp.2022.154179.
[65] Lin T-C, Yang C-H, Cheng L-H, et al. Fibronectin in cancer: friend or foe. Cells. 2019;9(1):27. doi: 10.3390/cells9010027.
[66] Deng B, Zhao Z, Kong W, et al. Biological role of matrix stiffness in tumor growth and treatment. J Transl Med. 2022;20(1):540. doi: 10.1186/s12967-022-03768-y.
[67] Huet-Calderwood C, et al. Fibroblasts secrete fibronectin under lamellipodia in a microtubule- and myosin II-dependent fashion. J Cell Biol. 2023;222(2).
[68] Levental KR, Yu H, Kass L, et al. Matrix crosslinking forces tumor progression by enhancing integrin signaling. Cell. 2009;139(5):891–906. doi: 10.1016/j.cell.2009.10.027.
[69] Winkler J, Abisoye-Ogunniyan A, Metcalf KJ, et al. Concepts of extracellular matrix remodelling in tumour progression and metastasis. Nat Commun. 2020;11(1):5120. doi: 10.1038/s41467-020-18794-x.
[70] Peters JH, Sporn LA, Ginsberg MH, et al. Human endothelial cells synthesize, process, and secrete fibronectin molecules bearing an alternatively spliced type III homology (ED1). Blood. 1990;75(9):1801–1808. doi: 10.1182/blood.V75.9.1801.bloodjournal7591801.
[71] Howard BV, Macarak EJ, Gunson D, et al. Characterization of the collagen synthesized by endothelial cells in culture. Proc Natl Acad Sci USA. 1976;73(7):2361–2364. doi: 10.1073/pnas.73.7.2361.
[72] Cialdai F, Risaliti C, Monici M. Role of fibroblasts in wound healing and tissue remodeling on earth and in space. Front Bioeng Biotechnol. 2022;10:958381. doi: 10.3389/fbioe.2022.958381.
[73] Talbott HE, Mascharak S, Griffin M, et al. Wound healing, fibroblast heterogeneity, and fibrosis. Cell Stem Cell. 2022;29(8):1161–1180. doi: 10.1016/j.stem.2022.07.006.
[74] Zhang C, Li H, Jiang M, et al. Hypoxic microenvironment promotes dermal fibroblast migration and proliferation via a BNIP3-autophagy pathway. FEBS J. 2024;291(2):358–375. doi: 10.1111/febs.16985.
[75] Newman AC, Nakatsu MN, Chou W, et al. The requirement for fibroblasts in angiogenesis: fibroblast-derived matrix proteins are essential for endothelial cell lumen formation. Mol Biol Cell. 2011;22(20):3791–3800. doi: 10.1091/mbc.E11-05-0393.
[76] Yu S, Wang S, Wang X, et al. The axis of tumor-associated macrophages, extracellular matrix proteins, and cancer-associated fibroblasts in oncogenesis. Cancer Cell Int. 2024;24(1):335. doi: 10.1186/s12935-024-03518-8.